

A statistical theory of electronic degrees of freedom in wave packet molecular dynamics

Daniel Plummer,^{1,*} Pontus Svensson,^{1,2} Wiktor Jasniak,¹ Patrick Hollebon,³ Sam M. Vinko,¹ and Gianluca Gregori¹

¹*Department of Physics, University of Oxford, UK*

²*Helmholtz-Zentrum Dresden-Rossendorf (HZDR), D-01328 Dresden, Germany*

³*AWE, Aldermaston, Reading, Berkshire RG7 4PR, UK*

(Dated: February 3, 2026)

We derive statistical distributions for the degrees of freedom in wave packet molecular dynamics models. Specifically, a theory is developed for the width distributions of Gaussian wavepackets in both isotropic and anisotropic formulations. The resulting distribution functions show good agreement with molecular dynamics data under warm dense matter conditions, providing practical guidance for constraining the confining potential, an empirical parameter in the model. We also discuss how these distributions influence the resulting effective Coulomb interactions.

Keywords: Wave Packet Molecular Dynamics, Statistical Mechanics, Warm Dense Matter

I. INTRODUCTION

The modeling of many-body quantum systems from first principles presents a formidable challenge. A particularly demanding regime is so-called warm dense matter (WDM) [1], which has attracted significant interest due to its appearance in both planetary and solar interiors [2–4], and its formation during the compression phase of an inertial confinement fusion capsule [5]. While exact wavefunction propagation is computationally unfeasible for many-particle systems, finite-temperature quantum-statistical approaches such as path integral Monte Carlo (PIMC) can provide a diverse range of equilibrium properties [6–9]. Alternatively, self-consistent-field methods, typically for the electron subsystem, can be employed. The most prominent example being the plethora of density functional theory (DFT) based approaches which, once an approximation for the exchange-correlation functional is made, provide access to many static and dynamic properties [1, 5, 8–11]. Furthermore, to probe low-frequency ion features over large length scales – where direct simulation is impractical – effective ion potentials may be extracted through various approaches, including neural networks [12–14]. Alternatively, simple pair potentials may be used in the semi-classical regime [15–17].

Wave packet molecular dynamics (WPMD) is an alternative approach based on restricting the electronic wave function to yield a computationally feasible method [18–22]. This scheme enables simulations involving many thousands of particles, significantly reducing finite-size effects compared to PIMC- and DFT-based methods. Such an approach could also be complementary to the more established methods for a variety of additional reasons. In equilibrium, WPMD captures the joint evolution of electrons and ions over long timescales, enabling direct study of inter-species coupling beyond the Born–Oppenheimer approximation. In addition to dynamic

electron properties [23, 24], this allows electron-ion collisional transport to be directly modeled [25]. Furthermore, WPMD has been employed in an ongoing debate regarding the effect of electronic fluctuations on both diffusive and acoustic ion modes in dense plasma [26–28]. The method has also been extended to include bound-state wavefunctions [29, 30], which allowed the latter reference to extract the self-consistent ionization states using the scheme in Ref. [31]. In the nonequilibrium context, the method was used to study the relaxation of a two-temperature electron-proton plasma and yielded slow relaxation rates when compared with semi-classical models [32].

However, care must be taken to ensure that the restricted functional form of the electronic wavefunction does not lead to unphysical behaviour. A primary example is the confining potential, which controls the electron extent and hence regulates many properties of the model [24, 30, 33]. The purpose of this work is to highlight how the statistical distribution of the additional electron degrees of freedom in WPMD may be predicted from the Hamiltonian structure of the underlying equations. This provides a practical means to assess the effect of the confining potential. Here, we focus on the statistical properties of WPMD using a Gaussian ansatz, which has been widely applied to the study of warm dense matter and partially ionized plasmas.

II. GAUSSIAN WAVEPACKET ANSÄTZE

We employ an anisotropic Gaussian wavepacket ansatz developed in Ref. [34], and subsequently used in Refs. [23, 30]. The key results are briefly recalled for the purposes of this work. We start with N classical protons and N quantum electrons, and employ the mixed quantum-classical approach of Ehrenfest dynamics [35]. For hydrogen ions, the resulting evolution is dictated by the

* daniel.plummer@physics.ox.ac.uk

following Ehrenfest Hamiltonian,

$$\mathcal{H} = \sum_I \frac{\mathbf{P}_I^2}{2M_I} + \frac{e^2}{4\pi\epsilon_0} \sum_{I < J} \frac{1}{|\mathbf{R}_I - \mathbf{R}_J|} + \mathcal{H}^{\text{eff}}. \quad (1)$$

Here M_I , \mathbf{R}_I and \mathbf{P}_I denote the mass, position and momentum of the I^{th} ion respectively; additionally e is the electron charge and ϵ_0 is the permittivity of free space. The corresponding Hamiltonian equations of motion are

$$\frac{d\mathbf{R}_I}{dt} = \frac{\mathbf{P}_I}{M_I} \quad ; \quad \frac{d\mathbf{P}_I}{dt} = -\frac{\partial \mathcal{H}}{\partial \mathbf{R}_I}. \quad (2)$$

The effective Hamiltonian representing the quantum subsystem is the expectation value of the electron Hamiltonian with respect to the many-body wavefunction $|\Psi\rangle$,

$$\mathcal{H}^{\text{eff}} = \langle \Psi | \hat{H}_e(\{\mathbf{R}_I\}) | \Psi \rangle, \quad (3)$$

where \hat{H}_e is the electronic Hamiltonian operator. This operator depends parameterically on the ionic coordinates $\{\mathbf{R}_I\}$, and includes the electron kinetic energy together with all electron interaction terms. In Ehrenfest dynamics, $|\Psi\rangle$ spans the entire Hilbert space, and the ions evolve under forces obtained from the instantaneous expectation value of the electronic Hamiltonian. This corresponds to a mean-field treatment, in which the nuclei experience the averaged influence of the electronic state rather than evolving on a single potential energy surface. In WPMD, $|\Psi\rangle$ is parameterized by a finite set of continuous parameters $\{q_\mu\}$ which define a manifold in the full Hilbert space. To distinguish this case we perform the replacement

$$|\Psi\rangle \rightarrow |Q(\{q_\mu\})\rangle \quad ; \quad \mathcal{H}^{\text{eff}} \rightarrow \mathcal{H}^{\text{WP}} = \langle Q | \hat{H}_e(\{\mathbf{R}_I\}) | Q \rangle, \quad (4)$$

where $|Q\rangle$ is the parameterized wavefunction with the explicit parameter dependence suppressed and \mathcal{H}^{WP} is the corresponding wavepacket Hamiltonian. The two restricted Gaussian wavefunctions studied in this work shall now be specified.

Anisotropic form: A Hartree product of single-particle Gaussian orbitals is chosen, each with the functional form

$$\langle \mathbf{x} | q_i \rangle = \mathcal{N} \exp \left[-(\mathbf{x} - \mathbf{r}_i)^T \mathbf{M}_i (\mathbf{x} - \mathbf{r}_i) + \frac{i}{\hbar} \mathbf{p}_i^T (\mathbf{x} - \mathbf{r}_i) \right] \quad (5)$$

where $\mathbf{r}_i, \mathbf{p}_i$ correspond to the expected position and momenta respectively, \mathcal{N} is a normalization factor [34] and \hbar is the reduced Planck's constant. The symmetric complex three-by-three shape matrix

$$\mathbf{M}_i = \frac{1}{4} \Sigma_i^{-1} - \frac{i}{\hbar} \Pi_i \quad (6)$$

is commonly decomposed into a real covariance part, Σ_i , which is positive definite with units of length squared, and a conjugate shape-momentum variable Π_i . Explicitly the electronic subsystem now depends on the real

parameters $\{\mathbf{r}_i, \mathbf{p}_i, \Sigma_i, \Pi_i\}_{i=1}^N$ where i labels an electron in the system. The equations of motions are of Hamiltonian form

$$\frac{d\mathbf{r}_i}{dt} = \frac{\partial \mathcal{H}^{\text{WP}}}{\partial \mathbf{p}_i} \quad ; \quad \frac{d\mathbf{p}_i}{dt} = -\frac{\partial \mathcal{H}^{\text{WP}}}{\partial \mathbf{r}_i} \quad (7)$$

for the vector degrees of freedom, while the matrix degrees of freedom have the following symmetrized Hamiltonian structure:

$$\begin{aligned} \frac{d}{dt} \Sigma_{i\beta\alpha} &= \frac{1}{2} \left(\frac{\partial \mathcal{H}^{\text{WP}}}{\partial \Pi_{i\alpha\beta}} + \frac{\partial \mathcal{H}^{\text{WP}}}{\partial \Pi_{i\beta\alpha}} \right) \\ \frac{d}{dt} \Pi_{i\alpha\beta} &= -\frac{1}{2} \left(\frac{\partial \mathcal{H}^{\text{WP}}}{\partial \Sigma_{i\alpha\beta}} + \frac{\partial \mathcal{H}^{\text{WP}}}{\partial \Sigma_{i\beta\alpha}} \right), \end{aligned} \quad (8)$$

where $\Sigma_{i\alpha\beta} = [\Sigma_i]_{\alpha\beta}$ is the α, β component of the symmetric width matrix and, similarly, $\Pi_{i\alpha\beta} = [\Pi_i]_{\alpha\beta}$ is a component of the conjugate width-momentum matrix, both corresponding to the i -th electron.

Isotropic form: The isotropic case is also studied. Constraining the matrices to

$$\Sigma_i = \lambda_i \mathbf{I} \quad ; \quad \Pi_i = \pi_i \mathbf{I}, \quad (9)$$

where \mathbf{I} is the identity matrix and λ_i, π_i are real scalars, gives the isotropic state

$$\langle \mathbf{x} | g_i \rangle = \mathcal{N} \exp \left[-m_i (\mathbf{x} - \mathbf{r}_i)^2 + \frac{i}{\hbar} \mathbf{p}_i^T (\mathbf{x} - \mathbf{r}_i) \right], \quad (10)$$

with the complex width variable

$$m_i = \frac{1}{4\lambda_i} - \frac{i}{\hbar} \pi_i. \quad (11)$$

While the equations of motion for the expected position \mathbf{r}_i and expected momentum \mathbf{p}_i remain with the same form given in Eq. (7), the evolution equations for the internal degrees of freedom reduce to

$$\frac{d\lambda_i}{dt} = \frac{1}{3} \frac{\partial \mathcal{H}^{\text{WP}}}{\partial \pi_i} \quad ; \quad \frac{d\pi_i}{dt} = -\frac{1}{3} \frac{\partial \mathcal{H}^{\text{WP}}}{\partial \lambda_i}. \quad (12)$$

The factor of three is a direct result of transitioning from a three-by-three matrix to a single variable in Eq. (9). This form is closely related to the isotropic Gaussian first used to model dense plasmas [20], and subsequently studied by many authors.

A. Additional potentials

In WPMD models for dense plasma, additional effective potentials are typically included, see, e.g., Refs. [20, 34, 36]. Firstly, so-called *Pauli potentials* which are additional two-body potentials motivated by a pairwise truncation of the antisymmetrization operator [19, 20], partially addressing the limitation of the Hartree product in the restricted wavefunction. We employ Pauli potentials in this work, although directly antisymmetrized

wavefunctions have previously been considered [21]. Alternative schemes inspired by exchange-correlation energy approximations from DFT have also been investigated [22, 37]. Secondly, a confining potential is used to enforce localized Gaussian wavepackets, which is standard in high temperature applications of WPMD. This is what we focus on in the present work. An additional potential energy operator is added to the electronic Hamiltonian [23, 30]:

$$\hat{V} = \frac{A}{2} \sum_i \hat{W}_i = \frac{A}{2} \sum_i (\hat{\mathbf{x}}_i - \langle \hat{\mathbf{x}}_i \rangle)^2 \quad (13)$$

where $\hat{\mathbf{x}}_i$ denotes the position operator of the i -th electron and $\langle \hat{\mathbf{x}}_i \rangle$ denotes its expectation value. We have also defined the width-squared operator \hat{W}_i , which shall be used to characterize the extent of the electron wavefunction. As shall be demonstrated, adjusting A modulates the distribution of the width variables (Σ_i or λ_i) in the model. This changes the effective Coulomb interactions and resulting structural properties [30]. An alternative scheme based on a global confining potential to impose reflecting wall boundary conditions has also been studied in Refs [22, 38]. We shall briefly comment how to extend the method presented here to this scheme in Sec. III A.

III. STATISTICAL THEORY FOR THE WIDTH DISTRIBUTION

In this section we develop a statistical theory for the internal degrees of freedom based on the non-interacting limit. Specifically, we assume single-particle contributions to the total energy are dominant and that the presence of width-dependent Coulomb and Pauli interactions have a small effect on the internal degrees of freedom. This assumption is correct for sufficiently weakly-coupled systems. More generally, its validity may be assessed by comparison to interacting molecular dynamics simulations, as performed in Sec IV. Of course, at sufficiently strongly-coupled conditions, the presence of interactions will perturb the width distribution away from the ideal case. Finally, we note that width distributions have been discussed for isotropic wavepackets in previous works, see e.g. Refs [32, 37–40], but not directly predicted.

A. Anisotropic case

In an ideal gas of anisotropic wavepackets, the Hamiltonian is a sum over kinetic terms and confining potential terms:

$$\mathcal{H}^{\text{WP}} = \sum_i \left(\mathcal{T}_i + \frac{A}{2} \text{Tr} \{ \Sigma_i \} \right). \quad (14)$$

As discussed in the previous section, the final term represents the confining potential with empirical strength A . This term arises from evaluating the expectation value of

Eq. (13) for an anisotropic Gaussian wavefunction, given in Eq. (5). Without this term, the partition function diverges due to infinite wavepacket spread [33]. If, instead, a global confining potential is used, then the final term in this equation should be replaced by an external, position- and shape-dependent potential. For anisotropic wavepackets the kinetic energy is given by [34]

$$\mathcal{T}^{\text{ani}} = \frac{\mathbf{p}^2}{2m} + \frac{2}{m} \text{Tr} \{ \Pi \Sigma \Pi \} + \frac{\hbar^2}{8m} \text{Tr} \{ \Sigma^{-1} \} \quad (15)$$

where m is the electron mass and the particle index has been suppressed. In a non-interacting system with classical Hamiltonian equations, the many-body distribution function factorizes into a set of N single-particle distribution functions:

$$f_1(\mathbf{p}, \Sigma, \Pi) = \frac{1}{Z_1} \exp \left(-\beta \mathcal{T} + \frac{A}{2} \text{Tr} \{ \Sigma \} \right), \quad (16)$$

where $\beta = 1/(k_B T)$ is the inverse temperature and Z_1 is the single-particle partition function associated to the extended phase space of the model. Note that no closed-form expression is readily available for Z_1 . To study the resulting distribution over widths, we proceed by integrating the single-particle distribution function over both the position and momentum degrees of freedom to find a marginal distribution in terms of the Σ matrix:

$$f_{\Sigma}^{\text{ani}}(\Sigma) = \int d^3 \mathbf{r} \int d^3 \mathbf{p} \int d^6 \Pi f_1(\mathbf{p}, \Sigma, \Pi). \quad (17)$$

The Σ matrix is symmetric, and therefore admits an eigendecomposition, $\Sigma = \Lambda D \Lambda^T$, where $\Lambda \in \mathbb{R}^{3 \times 3}$ is an orthogonal matrix of eigenvectors ($\Lambda^T \Lambda = I$) and $D = \text{diag}(\lambda_1, \lambda_2, \lambda_3)$ is a diagonal matrix of eigenvalues. Therefore, upon making the following change of variables, $\Pi' = \Lambda^T \Pi \Lambda$, the trace may be written as $\text{Tr}(\Pi \Sigma \Pi) = \text{Tr}(\Pi' D \Pi')$. Orthogonal transformations preserve volume and so the integration measure remains unchanged, i.e. $d^6 \Pi = d^6 \Pi'$, and the total distribution becomes

$$f_{\Sigma}^{\text{ani}}(\Sigma) = \mathcal{Z} \exp \left[-\beta \left(\frac{\hbar^2}{8m} \text{Tr} \{ \Sigma^{-1} \} + \frac{A}{2} \text{Tr} \{ \Sigma \} \right) \right] I_1, \quad (18)$$

where \mathcal{Z} is used henceforth as a normalization constant that is redefined as necessary to absorb prefactors. The last term is the following integral:

$$I_1 = \int \exp \left[-\beta \frac{2}{m} \text{Tr} \{ \Pi' D \Pi' \} \right] d^6 \Pi'. \quad (19)$$

The matrix Π' is symmetric, so the trace can be expanded accordingly:

$$\text{Tr}(\Pi' D \Pi') = \sum_{p=1}^3 \lambda_p (\Pi'_{pp})^2 + 2 \sum_{1 \leq p < q \leq 3} (\lambda_p + \lambda_q) (\Pi'_{pq})^2.$$

Therefore the integral factorizes into six independent Gaussian integrals. Performing these integrals yields

$$f_{\Sigma}^{\text{ani}}(\Sigma) = \mathcal{Z} \left(\prod_{p=1}^3 \frac{1}{\sqrt{\lambda_p}} \right) \left(\prod_{1 \leq p < q \leq 3} \frac{1}{\sqrt{\lambda_p + \lambda_q}} \right) \exp \left[-\beta \left(\frac{\hbar^2}{8m} \text{Tr} \{ \Sigma^{-1} \} + \frac{A}{2} \text{Tr} \{ \Sigma \} \right) \right]. \quad (20)$$

Since the shape matrix Σ is symmetric, it has six degrees of freedom. We wish to study the distribution of widths, which depend on the three eigenvalues of Σ , denoted by $\lambda_1, \lambda_2, \lambda_3$. To isolate these, we express the integral in terms of these three variables and integrate over the three rotation variables μ_1, μ_2, μ_3 which parameterize the possible orientation of the eigenbasis. It is possible to show that the Jacobian associated to this transformation is [41]

$$\mathcal{J}(\lambda_1, \lambda_2, \lambda_3, \mu_1, \mu_2, \mu_3) = \prod_{1 \leq p < q \leq 3} |\lambda_p - \lambda_q| g(\mu_1, \mu_2, \mu_3), \quad (21)$$

where g is the distribution function of the μ degrees of freedom. After integrating over the rotational degrees of freedom, the marginal distribution function over the eigenvalues is

$$f_{\lambda}^{\text{ani}}(\lambda_1, \lambda_2, \lambda_3) = \mathcal{Z} \left(\prod_{p=1}^3 \frac{1}{\sqrt{\lambda_p}} \right) \left(\prod_{1 \leq p < q \leq 3} \frac{|\lambda_p - \lambda_q|}{\sqrt{\lambda_p + \lambda_q}} \right) \exp \left[-\beta \left(\frac{\hbar^2}{8m} \sum_{p=1}^3 \frac{1}{\lambda_p} + \frac{A}{2} \sum_{p=1}^3 \lambda_p \right) \right]. \quad (22)$$

To characterize the resulting distribution we sample directly from the joint distribution of the eigenvalues $\lambda = (\lambda_1, \lambda_2, \lambda_3)$ defined in Eq. (22). From each set of sampled eigenvalues we calculate the widths

$$\sigma_p = \sqrt{\lambda_p} \quad \text{for } p = 1, 2, 3, \quad (23)$$

which provide a more natural physical interpretation. In order to characterize the statistics of these widths we consider the distribution of an individual width, denoted P_{σ}^{ani} , obtained by pooling all σ_i values across samples. Additionally, to measure the total wavepacket extent, we define the root-mean-squared (RMS) width as

$$\bar{\sigma} = \sqrt{\frac{1}{3} \langle \hat{W} \rangle} = \sqrt{\frac{1}{3} (\sigma_1^2 + \sigma_2^2 + \sigma_3^2)}, \quad (24)$$

where the first equality is the general definition in terms of the width-squared operator defined in Eq. (13). Evaluating the state average for the specific case of anisotropic wavepackets yields the second equality. The marginal probability distribution of the RMS width $\bar{\sigma}$ is denoted $P_{\bar{\sigma}}^{\text{ani}}$. These two marginal distributions capture, respectively, the typical fluctuations of a single component and the collective behavior of the total width.

B. Isotropic case

The equivalent Hamiltonian for an ideal gas of isotropic wavepackets is

$$\mathcal{H}^{\text{WP}} = \sum_i \left(\mathcal{T}_i + \frac{3A}{2} \lambda_i \right), \quad (25)$$

which includes the state average of the confining potential using the isotropic wavepacket form given in Eq. (10). For isotropic wavepackets, the kinetic energy is

$$\mathcal{T}^{\text{iso}} = \frac{\mathbf{p}^2}{2m} + \frac{6}{m} \pi^2 \lambda + \frac{3\hbar^2}{8m\lambda}, \quad (26)$$

where the particle index is suppressed. Following the same procedure as the previous subsection and integrating over all momentum-like degrees of freedom gives the following distribution function over λ ,

$$f_{\lambda}^{\text{iso}}(\lambda) = \sqrt{\frac{3A\beta}{2\pi\lambda}} \exp \left[-\beta \left(\frac{3\hbar^2}{8m\lambda} + \frac{3}{2}A\lambda - \frac{3}{2}\sqrt{A} \right) \right]. \quad (27)$$

Here the normalization factor has been explicitly calculated. The width metric employed for the anisotropic case can also be applied to the isotropic case. Specifically, we define the isotropic width variable

$$\sigma = \sqrt{\frac{1}{3} \langle \hat{W} \rangle} = \sqrt{\lambda}, \quad (28)$$

where the second equality is evaluated for the isotropic Gaussian, Eq. (10), in contrast to the anisotropic wavefunction used to evaluate the state average appearing in the second equality of Eq. (24). The width variable σ has the following marginal distribution function:

$$f_{\sigma}^{\text{iso}}(\sigma) = 2\sigma f_{\lambda}^{\text{iso}}(\sigma^2), \quad (29)$$

which is the isotropic equivalent to the marginal probability of the averaged width $P_{\bar{\sigma}}^{\text{ani}}$. It is also possible to find a closed-form expression for the mean width of the distribution,

$$\begin{aligned} \langle \sigma \rangle^{\text{iso}} &= \int \sigma f_{\sigma}^{\text{iso}}(\sigma) d\sigma \\ &= \sqrt{\frac{3\hbar^2\beta}{2\pi m}} \exp \left[\frac{3}{2}\beta\sqrt{A} \right] K_1 \left[\frac{3}{2}\hbar\beta\sqrt{\frac{A}{m}} \right] \end{aligned} \quad (30)$$

where $\langle \cdot \rangle^{\text{iso}}$ denotes the statistical average with respect to the isotropic width distribution function and $K_{\alpha}[\cdot]$ denotes the modified Bessel function of the second kind of

order α . Additionally, the maximum of the distribution, calculated with

$$\frac{\partial f_\sigma^{\text{iso}}}{\partial \sigma} = 0, \quad (31)$$

gives the isotropic modal width:

$$\text{mode}(\sigma) = \left(\frac{\hbar^2}{4mA} \right)^{1/4}, \quad (32)$$

which is equivalent to equating shape kinetic energy and confining potential terms, and has previously been used to ascribe an approximate electronic lengthscale to the confining strength in WPMD [30, 42].

IV. COMPARISON AGAINST INTERACTING MOLECULAR DYNAMICS DATA

A. Numerical Details

1. Molecular dynamics

We now compare the non-interacting theory developed in the previous section with fully interacting molecular dynamics data for warm dense hydrogen. The full model being employed, including confining and Pauli potentials, corresponds to the fully ionized model specified in Ref. [30]. The long-range Coulombic interactions are computed in k-space according to Ewald treatment in Ref. [34]. A timestep of 5×10^{-5} fs and real-space cutoff for Pauli interactions of $12 a_0$ ensures stable energy conservation. Results are presented for a Brückner density parameter of $r_s = 2$ and a quantum degeneracy parameter of $\theta = k_B T/E_F = 1$, where E_F is the Fermi energy. Width distribution data is time-averaged over snapshots that encompass a 25 fs period.

2. Markov Chain Monte Carlo

To compute the width distributions in the non-interacting statistical theory of anisotropic wavepackets, we sample $\boldsymbol{\lambda} = (\lambda_1, \lambda_2, \lambda_3)$ from Eq. (22) using an MCMC sampling routine. Specifically, to generate samples from the target density we employ the *random-walk Metropolis* algorithm [43–45]. At each step the algorithm proposes a move in parameter space and then accepts or rejects it according to the Metropolis rule. Concretely, starting from an initial state $\boldsymbol{\lambda}^{(0)}$, the algorithm iterates the following steps:

1. Propose a new point $\boldsymbol{\lambda}^{\text{prop}} = \boldsymbol{\lambda}^{(t)} + \boldsymbol{\eta}$, where $\boldsymbol{\eta} \sim \mathcal{N}(\mathbf{0}, \sigma^2 I)$.
2. Compute the log of the unnormalized target density at the proposal and the current state, and form the acceptance probability

$$\alpha = \min \left\{ 1, \exp \left[\log f_{\boldsymbol{\lambda}}^{\text{ani}}(\boldsymbol{\lambda}^{\text{prop}}) - \log f_{\boldsymbol{\lambda}}^{\text{ani}}(\boldsymbol{\lambda}^{(t)}) \right] \right\}.$$

3. With probability α , accept the proposal and set $\boldsymbol{\lambda}^{(t+1)} = \boldsymbol{\lambda}^{\text{prop}}$; otherwise, keep the current state $\boldsymbol{\lambda}^{(t+1)} = \boldsymbol{\lambda}^{(t)}$.

Evaluating the density in log space prevents numerical underflow and converts products into sums, which is more numerically stable.

The Gaussian proposal width σ is varied to yield a reasonable acceptance rate of around 0.3. Each run consists of 2×10^6 iterations, with the first 10^5 discarded as burn-in and every 20th sample retained (thinning) for analysis. The retained states are transformed to widths $\sigma_i = \sqrt{\lambda_i}$, from which we construct the single-particle distribution P_σ^{ani} and the averaged distribution P_σ^{ani} . Performing multiple independent runs confirmed consistent acceptance rates and stable estimates of the marginal distributions.

B. Model comparison

Fig. 1 shows the sampled distributions compared to the interacting molecular dynamics simulations specified in the previous subsection for different values of the confining strength A . The agreement between the classical statistical theory and interacting width distributions is remarkable. Additionally, a shoulder feature is observed in the tail of each distribution, as indicated by the arrows in Figure 1. This feature arises due to the eigenvalue difference term, $\prod_{1 \leq p < q \leq 3} |\lambda_q - \lambda_p|$, present in the marginal distribution over eigenvalues, which appears in the second product of Eq. (22). This *eigenvalue repulsion* suppresses configurations with a similar spatial extent in each diagonalized spatial dimension, because fewer distinct covariance matrices Σ correspond to such points. This term directly originates from the rotational degrees of freedom in the model, which provide additional relaxation pathways. The equivalence between the width distribution from the statistical theory and from the interacting system provides direct evidence that the effective interactions of the model are mediated by the classical statistics of the wavepacket Hamiltonian \mathcal{H}^{WP} . To demonstrate this point we plot effective interparticle interactions in Fig. 2. These interactions are computed from the Coulomb interactions of an isotropic Gaussian with a width given by the mean of the corresponding distributions in Fig. 1. For narrow wavepackets, the interparticle Coulomb interaction is greater at smaller separations given that the charge distribution is more localized. While for larger separations with respect to the wavepacket width, the pair potentials asymptote to the Coulomb potential. At this condition, full ionization is expected, and the effect of interactions has little impact on the width PDFs. A comparison between the isotropic and anisotropic restricted wavefunctions is presented in Fig. 3. Panel (a) shows the isotropic distribution $f_\sigma(\sigma)$ computed with both MD and MCMC techniques, alongside the probability distribution for the average width of an isotropic wavepacket

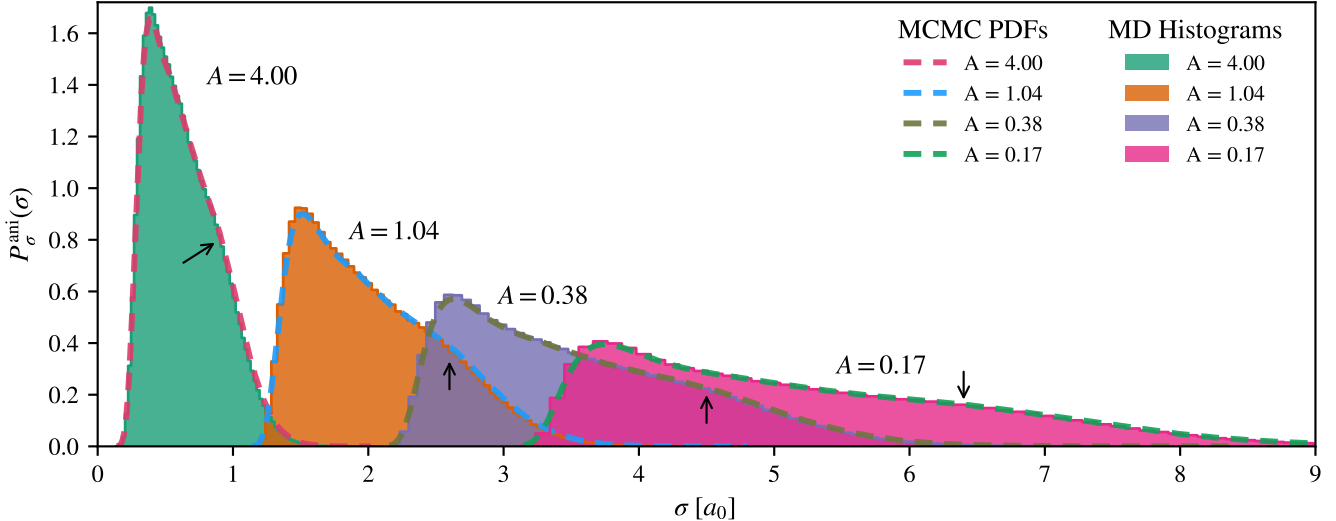


FIG. 1. Marginal width distribution functions for an anisotropic plasma at $r_s = 2$ and $\theta = 1$ for different confining potentials. Excluding the $A = 4.00 \text{ Ha}/a_0^2$ case, each curve is shifted by $1 a_0$ relative to the curve to its left for clarity. The histograms correspond to molecular dynamics (MD) results in the microcanonical ensemble, while the dashed lines correspond to Markov Chain Monte Carlo (MCMC) sampling of Eq. (22). Arrows indicate the shoulder feature discussed in the main text. The simulations are performed within a cubic box of side length $L = 52.5 a_0$. Hartree atomic units are used in the legend.

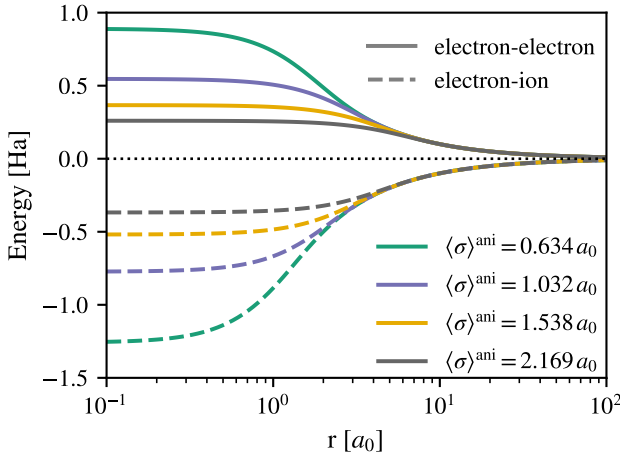


FIG. 2. Effective interparticle Coulomb interactions based on the mean width of the distributions plotted in Fig. 1.

$P_{\bar{\sigma}}^{\text{ani}}$. For an equivalent confining potential, the average extent of the anisotropic wavepacket is significantly larger. Panel (b) depicts the corresponding marginal distribution over individual width variables, which exhibits a prominent tail in the width distribution extending beyond $6 a_0$ and shoulder feature. Fig. 3 also demonstrates that the width of each anisotropic wavepacket is underestimated by the mode of the isotropic distribution. While emphasising the role of the underlying classical statistics, this comparison elucidates the difference in the two restricted wavefunctions. The isotropic wavefunctions are considerably more localized for a given confining potential.

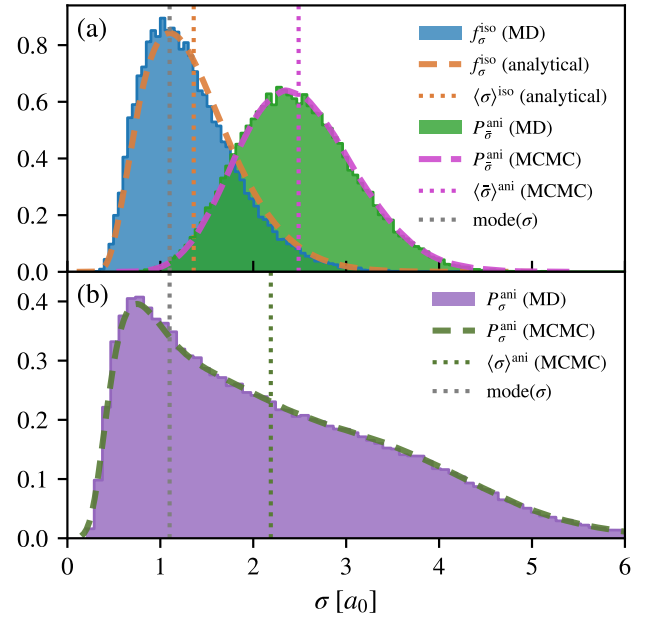


FIG. 3. Comparison between isotropic and anisotropic width distribution functions at $r_s = 2, \theta = 1$ for a confining potential of $A = 0.17 \text{ Ha}/a_0^2$. (a) Average width distribution functions for the isotropic and anisotropic models. (b) Distribution of individual width variables in the anisotropic model. The grey dashed line indicates the modal width of the isotropic model given by Eq. (32). The mean values of each distribution are also plotted, with the isotropic case given by Eq. (30), and the anisotropic case calculated numerically.

tial. This is likely explained by additional rotational degrees of freedom present in the anisotropic wavepacket ansatz that provide additional relaxation pathways in the dynamics and manifests as eigenvalue repulsion. The stronger localization in the isotropic ansatz for a given confining strength means it will have stronger electron-electron and electron-ion interactions, explaining weaker correlations observed for the anisotropic ansatz in a previous comparison [34], albeit for a different form of the confining potential.

V. DISCUSSION

WPMD-based simulations can capture the concurrent time evolution of thousands of coupled ions and electrons. However, applications in plasma physics require the use of a confining potential to appropriately constrain the electron widths. In this work, we have presented a method by which the effect of the confining potential can be predicted *a priori* for both isotropic and anisotropic variants of WPMD. From a practical perspective, this may allow confinement strength heuristics, such as those discussed in Refs [33, 42], to be developed and then applied, without the need to explicitly scan the parameter using molecular dynamics simulations to find a suitable choice, as was required in Ref. [31]. Additionally, we have investigated the distribution of electronic widths within a classical statistical theory. The comparison of two wavepacket models reveals that, even under equivalent confining potentials, they exhibit different mean widths and therefore different effective Coulomb interactions. This finding accounts for the structural differences previously reported between these models in the warm dense matter regime [34]. The results presented here could also be extended to the case of a global external confining potential and therefore used to predict its impact on the equilibrium density profile [22].

From a theoretical perspective, we have demonstrated that the distribution of variables in wavepacket models is closely connected to the statistical properties of the underlying classical Hamiltonian \mathcal{H}^{WP} . For the model to yield correct effective pairwise interactions—which are known from quantum statistical considerations to be

Coulomb-like at large separations and finite at small separations in weakly-coupled, fully-ionized plasmas [15]—it should relax to a non-divergent width distribution. As $A \rightarrow 0$ in either the anisotropic or isotropic case, the average width diverges and the distribution functions themselves, Eqs. (22) and (27), become unnormalizable. This observation establishes the confining potential as an essential ingredient for enforcing the correct behaviour in weakly-coupled regimes. Similar models, such as those used for nuclear collisions, often address this feature by fixing the wavepacket width directly [46].

In fully ionized warm dense systems, as studied here, a significant fraction of the electrons are expected to be in spatially-extended states. However, a fully delocalized Gaussian wavepacket will effectively cease to interact with the system and has no mechanism to relocalize. Therefore, by regulating the model through picking an appropriate confining potential, physically meaningful results can be obtained [22, 23, 30].

ACKNOWLEDGMENTS

We are grateful for the use of computing resources provided by STFC Scientific Computing Department’s SCARF cluster. DP, PS, SMV and GG acknowledge support from AWE-NST UK via Oxford Centre for High Energy Density Science (OxCHEDs). PS acknowledges funding from the Oxford Physics Endowment for Graduates (OXPEG). S.M.V. acknowledges support from the UK EPSRC grant EP/W010097/1. The work of SMV and GG has received partial support from EPSRC and First Light Fusion under the AMPLIFI Prosperity partnership, grant no. EP/X025 373/1. The work by PS was partially supported by the European Research Council (ERC) under the European Union’s Horizon 2022 research and innovation programme (Grant agreement No. 101076233, “PREXTREME”). Views and opinions expressed are however those of the authors only and do not necessarily reflect those of the European Union or the European Research Council Executive Agency. Neither the European Union nor the granting authority can be held responsible for them.

-
- [1] J. Vorberger, F. Graziani, D. Riley, A. D. Baczewski, I. Baraffe, M. Bethkenhagen, S. Blouin, M. P. Böhme, M. Bonitz, M. Bussmann, A. Casner, W. Cayzac, P. Celiers, G. Chabrier, N. Chamel, D. Chapman, M. Chen, J. Clérouin, G. Collins, F. Coppari, T. Döppner, T. Dornheim, L. B. Fletcher, D. O. Gericke, S. Glenzer, A. F. Goncharov, G. Gregori, S. Hamel, S. B. Hansen, N. J. Hartley, S. Hu, O. A. Hurricane, V. V. Karasiev, J. J. Kas, B. Kettle, T. Kluge, M. D. Knudson, A. Kononov, Z. K. á, D. Kraus, A. Kritcher, S. Malko, G. Massacrier, B. Militzer, Z. A. Moldabekov, M. S. Murillo, B. Náglér, N. Nettelmann, P. Neumayer, B. K. Ofori-Okai, I. I. Oleynik, M. Preising, A. Pribram-Jones, T. Ramazanov, A. Ravasio, R. Redmer, B. Rethfeld, A. P. L. Robinson, G. Röpke, F. Soubiran, C. E. Starrett, G. Steinle-Neumann, P. A. Sterne, S. Tanaka, A. P. Thompson, S. B. Trickey, T. Vinci, S. M. Vinko, L. Wang, A. J. White, T. G. White, U. Zastrau, E. Zurek, and P. Tolias, Roadmap for warm dense matter physics (2025), arXiv:2505.02494 [physics.plasm-ph].
- [2] D. Saumon, S. Blouin, and P.-E. Tremblay, Current challenges in the physics of white dwarf stars, Physics Re-

- ports **988**, 1 (2022), current Challenges in the Physics of White Dwarf Stars.
- [3] J.-A. Hernandez, M. Bethkenhagen, S. Ninet, M. French, A. Benuzzi-Mounaix, F. Datchi, M. Guaraguaglini, F. Lefevre, F. Occelli, R. Redmer, T. Vinci, and A. Ravasio, Melting curve of superionic ammonia at planetary interior conditions, *Nature Physics* **19**, 1280 (2023).
- [4] T. Guillot, Interiors of giant planets inside and outside the solar system, *Science* **286**, 72 (1999).
- [5] S. X. Hu, L. A. Collins, T. R. Boehly, Y. H. Ding, P. B. Radha, V. N. Goncharov, V. V. Karasiev, G. W. Collins, S. P. Regan, and E. M. Campbell, A review on ab initio studies of static, transport, and optical properties of polystyrene under extreme conditions for inertial confinement fusion applications, *Physics of Plasmas* **25**, 056306 (2018).
- [6] T. Dornheim, S. Groth, and M. Bonitz, The uniform electron gas at warm dense matter conditions, *Physics Reports* **744**, 1 (2018).
- [7] T. Dornheim, Z. A. Moldabekov, K. Ramakrishna, P. Tollas, A. D. Baczewski, D. Kraus, T. R. Preston, D. A. Chapman, M. P. Böhme, T. Döppner, F. Graziani, M. Bonitz, A. Cangi, and J. Vorberger, Electronic density response of warm dense matter, *Physics of Plasmas* **30**, 032705 (2023).
- [8] M. Bonitz, J. Vorberger, M. Bethkenhagen, M. P. Böhme, D. M. Ceperley, A. Filinov, T. Grawne, F. Graziani, G. Gregori, P. Hamann, S. B. Hansen, M. Holzmann, S. X. Hu, H. Kählert, V. V. Karasiev, U. Kleinschmidt, L. Kordts, C. Makait, B. Militzer, Z. A. Moldabekov, C. Pierleoni, M. Preising, K. Ramakrishna, R. Redmer, S. Schwalbe, P. Svensson, and T. Dornheim, Toward first principles-based simulations of dense hydrogen, *Physics of Plasmas* **31**, 110501 (2024).
- [9] B. Militzer, F. González-Cataldo, S. Zhang, K. P. Driver, and F. m. c. Soubiran, First-principles equation of state database for warm dense matter computation, *Phys. Rev. E* **103**, 013203 (2021).
- [10] Z. Moldabekov, S. Schwalbe, M. P. Böhme, J. Vorberger, X. Shao, M. Pavanello, F. R. Graziani, and T. Dornheim, Bound-state breaking and the importance of thermal exchange-correlation effects in warm dense hydrogen, *Journal of Chemical Theory and Computation* **20**, 68 (2024).
- [11] A. Kononov, C.-W. Lee, T. P. dos Santos, B. Robinson, Y. Yao, Y. Yao, X. Andrade, A. D. Baczewski, E. Constantinescu, A. A. Correa, Y. Kanai, N. Modine, and A. Schleife, Electron dynamics in extended systems within real-time time-dependent density-functional theory, *MRS Communications* **12**, 1002 (2022).
- [12] M. Schörner, H. R. Rüter, M. French, and R. Redmer, Extending ab initio simulations for the ion-ion structure factor of warm dense aluminum to the hydrodynamic limit using neural network potentials, *Phys. Rev. B* **105**, 174310 (2022).
- [13] S. Kumar, H. Tahmasbi, K. Ramakrishna, M. Lokamani, S. Nikolov, J. Tranchida, M. A. Wood, and A. Cangi, Transferable interatomic potential for aluminum from ambient conditions to warm dense matter, *Phys. Rev. Res.* **5**, 033162 (2023).
- [14] K. Wünsch, J. Vorberger, and D. O. Gericke, Ion structure in warm dense matter: Benchmarking solutions of hypernetted-chain equations by first-principle simulations, *Phys. Rev. E* **79**, 010201(R) (2009).
- [15] A. V. Filinov, V. O. Golubnychiy, M. Bonitz, W. Ebeling, and J. W. Dufty, Temperature-dependent quantum pair potentials and their application to dense partially ionized hydrogen plasmas, *Phys. Rev. E* **70**, 046411 (2004).
- [16] J. N. Glosli, F. R. Graziani, R. M. More, M. S. Murillo, F. H. Streitz, M. P. Surh, L. X. Benedict, S. Hau-Riege, A. B. Langdon, and R. A. London, Molecular dynamics simulations of temperature equilibration in dense hydrogen, *Phys. Rev. E* **78**, 025401 (2008).
- [17] G. S. Demyanov and P. R. Levashov, Molecular dynamics of nondegenerate hydrogen plasma using improved kelbg pseudopotential with electron thermal de broglie wavelength correction, *Physics of Plasmas* **32**, 123901 (2025).
- [18] H. Feldmeier and J. Schnack, Molecular dynamics for fermions, *Rev. Mod. Phys.* **72**, 655 (2000).
- [19] P. E. Grabowski, A review of wave packet molecular dynamics, in *Frontiers and Challenges in Warm Dense Matter*, edited by F. Graziani, M. P. Desjarlais, R. Redmer, and S. B. Trickey (Springer International Publishing, Cham, 2014) pp. 265–282.
- [20] D. Klakow, C. Toepffer, and P.-G. Reinhard, Hydrogen under extreme conditions, *Physics Letters A* **192**, 55 (1994).
- [21] B. Jakob, P.-G. Reinhard, C. Toepffer, and G. Zwicknagel, Wave packet simulation of dense hydrogen, *Phys. Rev. E* **76**, 036406 (2007).
- [22] Y. Lavrinenko, P. R. Levashov, D. V. Minakov, I. V. Morozov, and I. A. Valuev, Equilibrium properties of warm dense deuterium calculated by the wave packet molecular dynamics and density functional theory method, *Phys. Rev. E* **104**, 045304 (2021).
- [23] P. Svensson, Y. Aziz, T. Dornheim, S. Azadi, P. Hollebon, A. Skelt, S. M. Vinko, and G. Gregori, Modeling of warm dense hydrogen via explicit real-time electron dynamics: Dynamic structure factors, *Phys. Rev. E* **110**, 055205 (2024).
- [24] I. V. Morozov and I. A. Valuev, Localization constraints in gaussian wave packet molecular dynamics of nonideal plasmas, *Journal of Physics A: Mathematical and Theoretical* **42**, 214044 (2009).
- [25] P. Svensson, P. Hollebon, D. Plummer, S. M. Vinko, and G. Gregori, Modeling of warm dense hydrogen via explicit real-time electron dynamics: Electron transport properties, *Phys. Rev. E* **111**, 045208 (2025).
- [26] R. A. Davis, W. A. Angermeier, R. K. T. Hermsmeier, and T. G. White, Ion modes in dense ionized plasmas through nonadiabatic molecular dynamics, *Phys. Rev. Res.* **2**, 043139 (2020).
- [27] Y. Yao, Q. Zeng, K. Chen, D. Kang, Y. Hou, Q. Ma, and J. Dai, Reduced ionic diffusion by the dynamic electron-ion collisions in warm dense hydrogen, *Physics of Plasmas* **28**, 012704 (2021).
- [28] W. A. Angermeier and T. G. White, An investigation into the approximations used in wave packet molecular dynamics for the study of warm dense matter, *Plasma* **4**, 294 (2021).
- [29] W. Ebeling and B. Militzer, Quantum molecular dynamics of partially ionized plasmas, *Physics Letters A* **226**, 298 (1997).
- [30] D. Plummer, P. Svensson, W. Jasniak, P. Hollebon, S. M. Vinko, and G. Gregori, Modeling partially-ionized dense plasma using wavepacket molecular dynamics (2025), arXiv:2510.27446 [physics.plasm-ph].
- [31] D. Plummer, P. Svensson, D. O. Gericke, P. Hollebon,

- S. M. Vinko, and G. Gregori, Ionization calculations using classical molecular dynamics, *Phys. Rev. E* **111**, 015204 (2025).
- [32] Q. Ma, J. Dai, D. Kang, M. S. Murillo, Y. Hou, Z. Zhao, and J. Yuan, Extremely low electron-ion temperature relaxation rates in warm dense hydrogen: Interplay between quantum electrons and coupled ions, *Phys. Rev. Lett.* **122**, 015001 (2019).
- [33] W. Ebeling, A. Filinov, M. Bonitz, V. Filinov, and T. Pohl, The method of effective potentials in the quantum-statistical theory of plasmas, *Journal of Physics A: Mathematical and General* **39**, 4309 (2006).
- [34] P. Svensson, T. Campbell, F. Graziani, Z. Moldabekov, N. Lyu, V. S. Batista, S. Richardson, S. M. Vinko, and G. Gregori, Development of a new quantum trajectory molecular dynamics framework, *Philosophical Transactions of the Royal Society A* **381** (2023).
- [35] D. Marx and J. Hutter, *Ab Initio Molecular Dynamics: Basic Theory and Advanced Methods* (Cambridge University Press, 2009).
- [36] J. T. Su and W. A. Goddard, Excited electron dynamics modeling of warm dense matter, *Phys. Rev. Lett.* **99**, 185003 (2007).
- [37] Y. S. Lavrinenko, I. V. Morozov, and I. A. Valuev, Wave packet molecular dynamics–density functional theory method for non-ideal plasma and warm dense matter simulations, *Contributions to Plasma Physics* **59**, e201800179 (2019).
- [38] Y. S. Lavrinenko, I. Morozov, and I. A. Valuev, Reflecting boundary conditions for classical and quantum molecular dynamics simulations of nonideal plasmas, *Contributions to Plasma Physics* **56**, 448 (2016).
- [39] D. Klakow, C. Toepffer, and P. Reinhard, Semiclassical molecular dynamics for strongly coupled Coulomb systems, *The Journal of Chemical Physics* **101**, 10766 (1994).
- [40] Y. S. Lavrinenko, I. V. Morozov, and I. A. Valuev, High performance wave packet molecular dynamics with density functional exchange-correlation term for non-ideal plasma simulations, *Journal of Physics: Conference Series* **1787**, 012043 (2021).
- [41] M. Mehta, *Random Matrices*, Pure and Applied Mathematics (Academic Press, 2004).
- [42] M. Knaup, P.-G. Reinhard, and C. Toepffer, Wave packet molecular dynamics simulations of hydrogen near the transition to a metallic fluid, *Contributions to Plasma Physics* **39**, 57 (1999).
- [43] N. Metropolis, A. Rosenbluth, M. Rosenbluth, A. Teller, and E. Teller, Equation of state calculations by fast computing machines, *J. Chem. Phys.* **21**, 1087 (1953).
- [44] W. Hastings, Monte carlo sampling methods using markov chains and their applications, *Biometrika* **57**, 97 (1970).
- [45] C. Robert and G. Casella, *Monte Carlo Statistical Methods*, 2nd ed. (Springer, 2004).
- [46] A. Ono and H. Horiuchi, Antisymmetrized molecular dynamics for heavy ion collisions, *Progress in Particle and Nuclear Physics* **53**, 501 (2004).